11048 *Inorg. Chem.* **2009**, *48*, 11048–11057
DOI: 10.1021/ic901291b

Inorganic Chemistry
Article

Synthesis, Structures, and Luminescent and Magnetic Properties of Ln−Ag Heterometal−Organic Frameworks

Xiao-Qing Zhao, Bin Zhao,* Shi Wei, and Peng Cheng*

Department of Chemistry, Nankai University, Tianjin 300071, People's Republic of China

Received July 4, 2009

A series of Ln−Ag heterometal−organic frameworks based on 4-hydroxylpyridine-2,6-dicarboxylic acid (H_3CAM) with formulas $\{LaAg_2(CAM)(HCAM)(H_2O)_2\}_n$ (**1**), $\{LnAg(HCAM)_2(H_2O)_3\}_n$ (Ln = Pr, **2**; Nd, **3**; Sm, **4**; Eu, **5**), and $\{LnAg_3(CAM)_2(H_2O)\}_n$ (Ln=Gd, **6**; Tb, **7**; Dy, **8**; Tm, **9**; Yb, **10**), have been synthesized with the hydrothermal reaction of $Ln(OH)_3$, Ag_2O, and H_3CAM at 160 °C. The single-crystal X-ray diffraction analyses reveal that three kinds of structures are exclusively governed by the size of lanthanide ions and the progression of structures is mainly ascribed to the lanthanide contraction effect. Compound **1** consists of a 3D network with an α-polonium-like Ag^+-homometallic net and helical La^{3+} chain. Compounds **2**−**5** display a 2D honeycomb-like structure with 18-membered $Ln_3Ag_3O_{12}$ motifs, and compounds **6**−**10** can be described as a sandwich-like 3D framework built of a 3D Ag^+-homometallic net and 2D Ln^{3+}−4^4 layer. In **4** (Sm), **5** (Eu), **7** (Tb), and **8** (Dy) samples, the efficient energy transfer from CAM to Ln(III) ions was observed, which results in the typical intense emissions of corresponding Ln(III) ions in the visible region, and the strongest emissions are $^4G_{5/2} \rightarrow {}^6H_{7/2}$ (602 nm), $^5D_0 \rightarrow {}^7F_2$ (614 nm), $^5D_4 \rightarrow {}^7F_5$ (548 nm), and $^4F_{9/2} \rightarrow {}^6H_{13/2}$ (576 nm) transitions. Variable-temperature magnetic susceptibility measurements of **6**−**10** show that the ferromagnetic interaction between gadolinium(III) ions appears in **6**, whereas the μ_{eff} values of **7**−**10** smoothly decrease on cooling. For the orbital contribution of Ln(III) ions, it is very difficult to determine the intrinsic magnetic interactions between Ln(III) ions.

Introduction

The design and construction of lanthanide-transition (f−d) heterometal−organic frameworks (HMOFs) is a rapidly growing field in coordination chemistry and supramolecular chemistry, owing to HMOFs' intriguing architectures and potential to fabricate solid-state materials with special physical properties, arising from the presence of two dissimilar metal ions.[1−7] For the disparate nature of two kinds of metal ions, the synthesis of f−d HMOFs has encountered many challenges, such as the choice of appropriate organic ligands that can coordinate with both metal ions, the competitive reactions between lanthanide and transition metal ions with organic ligands, and the variable and high coordination numbers with low stereochemical preference. A universal strategy for constructing f−d HMOFs is to assemble mixed metal ions with polydentate compartmental ligands containing both O and N donors, with respect to lanthanide ions having a high affinity for binding to hard donors like the O atom, whereas most transition metal ions prefer to coordinate to soft donors like the N atom. As expected, various HMOFs with fascinating structures and special properties have been synthesized on the basis of these ligands, offering different donors.[2,3] At the same time, HMOFs can also be assembled through metal ions coordinated to some other noncompartmental ligands only having O donor atoms, such as oxalic acid, phthalic acid, and 2,2′-oxidiacetic acid.[4] Among all sorts of HMOFs, the majority are associated with 4f−3d mixed metal ions, which gain much more attention compared to those with 4f−4d.[2−4]

*To whom correspondence should be addressed. Fax: +86-22-23502458. E-mail: zhaobin@nankai.edu.cn (B.Z.).

(1) (a) Sakamoto, M.; Manseki, K.; Okawa, H. *Coord. Chem. Rev.* **2001**, *219*−*221*, 379. (b) Plečnik, C. E.; Liu, S.; Shore, S. G. *Acc. Chem. Res.* **2003**, *36*, 499. (c) Singh, A.; Mehrotra, R. C. *Coord. Chem. Rev.* **2004**, *248*, 101. (d) Tanase, S.; Reedijk, J. *Coord. Chem. Rev.* **2006**, *250*, 2501. (e) Zhou, Y. F.; Hong, M. C.; Wu, X. T. *Chem. Commun.* **2006**, 135. (f) Cahill, C. L.; de Lill, D. E.; Frisch, M. *CrystEngComm* **2007**, *9*, 15.

(2) For example: (a) Imdert, D.; Cantuel, M.; Bünzli, J. C. G.; Bernardinelli, G.; Piguet, C. *J. Am. Chem. Soc.* **2003**, *125*, 15698. (b) Guillou, O.; Daiguebonne, C.; Camara, M.; Kerbellec, N. *Inorg. Chem.* **2006**, *45*, 8468. (c) Mori, F.; Nyui, T.; Ishida, T.; Nogami, T.; Choi, K. Y.; Nojiri, H. *J. Am. Chem. Soc.* **2006**, *128*, 1440. (d) Xiang, S. C.; Hu, S. M.; Sheng, T. L.; Fu, R. B.; Wu, X. T.; Zheng, X. D. *J. Am. Chem. Soc.* **2007**, *129*, 15114. (e) Kong, X. J.; Reng, Y. P.; Chen, W. X.; Long, L. S.; Zheng, Z. P.; Huang, R. B.; Zheng, L. S. *Angew. Chem., Int. Ed.* **2008**, *47*, 2398.

(3) (a) Zhao, B.; Cheng, P.; Dai, Y.; Cheng, C.; Liao, D. Z.; Yan, S. P.; Jiang, Z. H.; Wang, G. L. *Angew. Chem., Int. Ed.* **2003**, *42*, 934. (b) Zhao, B.; Cheng, P.; Chen, X. Y.; Cheng, C.; Shi, W.; Liao, D. Z.; Yan, S. P.; Jiang, Z. H. *J. Am. Chem. Soc.* **2004**, *126*, 3012. (c) Zhao, B.; Chen, X. Y.; Cheng, P.; Liao, D. Z.; Yan, S. P.; Jiang, Z. H. *J. Am. Chem. Soc.* **2004**, *126*, 15394. (d) Zhao, B.; Gao, H. L.; Chen, X. Y.; Cheng, P.; Shi, W.; Liao, D. Z.; Yan, S. P.; Jiang, Z. H. *Chem.—Eur. J.* **2006**, *12*, 149. (e) Zhao, X. Q.; Zhao, B.; Ma, Y.; Shi, W.; Cheng, P.; Jiang, Z. H.; Liao, D. Z.; Yan, S. P. *Inorg. Chem.* **2007**, *46*, 5832. (f) Gao, H. L.; Zhao, B.; Zhao, X. Q.; Song, Y.; Cheng, P.; Liao, D. Z.; Yan, S. P. *Inorg. Chem.* **2008**, *47*, 11057. (g) Zhao, B.; Chen, X. Y.; Chen, Z.; Shi, W.; Cheng, P.; Liao, D. Z.; Yan, S. P. *Chem. Commun.* **2009**, 3113.

 Published on Web 11/05/2009 © 2009 American Chemical Society

Furthermore, the 4f−4d series is mostly focused on Ln−Ru or Ln−polyoxometalate systems,[5,6] while those with Ln−Ag ones are still limited.[7,8]

The lanthanide complexes, especially with Sm^{3+}, Eu^{3+}, Tb^{3+}, and Dy^{3+} ions, always exhibit intense luminescence.[9] In fact, for the weak lanthanide f−f transitions, the photophysical properties of lanthanide complexes are markedly dependent on their environments, and emission is sensitized by energy transfer from a suitable adjacent chromophore, such as phenyl and pyridyl, which is called the "antenna effect".[10]

On the other hand, as the more commonly antiferromagnetic interactions observed in compounds with numerous paramagnetic centers are of less interest, lanthanide ions, which have large spin moments, are appealing for the preparation of magnetic materials with ferro- or ferrimagnetic coupling. Since the orbital contributions of most f electron pairs and the influence of the crystal field effects have to be considered, the analyses of magnetic interactions among Ln^{3+} ions become very difficult.[11] The Gd^{3+} ion, whose f−f spin−orbit coupling effect is absent in the first order (for the $^8S_{7/2}$ ground state of the $4f^7$ core), is the simplest but most nontrivial element, and the influence of the ligand field can be safely neglected. As a consequence, there are a lot of literature sources that investigate the magnetic interactions of gadolinium(III) complexes that have been reported.[12,13] Most of them exhibit weak antiferromagnetic coupling among gadolinium(III) ions,[12] while there are a few with ferromagnetic behavior.[13]

Chart 1. Structures of H_3CAM (left) and H_2PDA (right)

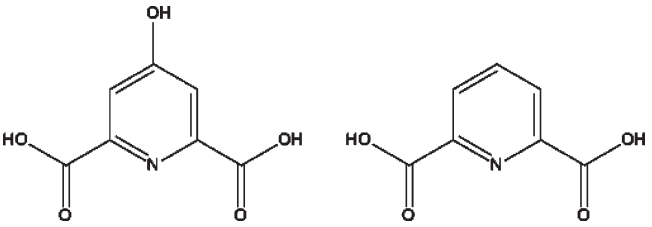

In previous work, we reported a series of porous 4f−3d (Ln−Mn/Co) HMOFs based on pyridine-2,6-dicarboxylic acid (H_2PDA),[3a−e] which exhibited interesting properties, such as a luminescent probe, radical adsorption, and ferromagnetic interaction. The corresponding 4f−4d systems (Ln−Ag) have also been obtained and show variable structure characters.[8] To investigate the effect of the hydroxyl group in the construction of HMOFs, 2D honeycomb-like Ln−Mn/Zn HMOFs have been generated under hydrothermal conditions with 4-hydroxylpyridine-2,6-dicarboxylic acid (H_3CAM) as a multifunctional ligand.[3d,f] H_3CAM combines the coordination geometry of H_2PDA and a hydroxyl group (Chart 1) and potentially provides many more coordination motifs than H_2PDA. As the successor to our previous work, herein, we report the syntheses and characterizations of a series of 4f−4d (Ln−Ag) HMOFs, $\{LnAg_2(CAM)(HCAM)(H_2O)_2\}_n$, $\{LnAg(HCAM)_2(H_2O)_3\}_n$ (Ln = Pr−Eu), and $\{LnAg_3(CAM)_2(H_2O)\}_n$ (Ln = Gd−Dy, Tm, Yb).

Experimental Section

Materials. All reagents and solvents employed were commercially available and used as received without further purification. Elemental analyses (C, H, and N) were performed on a Perkin-Elmer 240 CHN elemental analyzer. The fluorescent spectra were measured on a Varian Cary Eclipse Fluorescence spectrophotometer. Variable-temperature magnetic susceptibilities were measured on a Quantum Design MPMS-7 SQUID magnetometer. Diamagnetic corrections were applied with Pascal's constants for all of the constituent atoms.

Preparation of $\{LaAg_2(CAM)(HCAM)(H_2O)_2\}_n$ (1). A mixture of $La(OH)_3$ (0.2 mmol, 0.038 g), Ag_2O (0.2 mmol, 0.046 g), H_3CAM (0.6 mmol, 0.120 g), and H_2O (15 mL) was placed in a 25 mL Teflon-lined steel vessel and heated to 160 °C for 3 days

(4) (a) Decurtins, S.; Gross, M.; Schmalle, H. W.; Ferlay, S. *Inorg. Chem.* **1998**, *37*, 2443. (b) Baggio, R.; Garland, M. T.; Moreno, Y.; Pena, O.; Perec, M.; Spodine, E. *J. Chem. Soc., Dalton Trans.* **2000**, 2061. (c) Kahn, M. L.; Lecante, P.; Verelst, M.; Mathonière, C.; Kahn, O. *Chem. Mater.* **2000**, *12*, 3073. (d) Wang, Y.; Cheng, P.; Chen, J.; Liao, D. Z.; Yan, S. P. *Inorg. Chem.* **2007**, *46*, 4530. (e) Prasad, T. K.; Rajasekharan, M. V.; Costes, J. P. *Angew. Chem., Int. Ed.* **2007**, *46*, 2851.

(5) For example: (a) Miller, T. A.; Jeffery, J. C.; Ward, M. D.; Adams, H.; Pope, S. J. A.; Faulkner, S. *Dalton Trans.* **2004**, 1524. (b) Davies, G. M.; Pope, S. J. A.; Adams, H.; Faulkner, S.; Ward, M. D. *Inorg. Chem.* **2005**, *44*, 4656. (c) Yeung, W. F.; Lau, T. C.; Wang, X. Y.; Gao, S.; Szeto, L.; Wong, W. T. *Inorg. Chem.* **2006**, *45*, 6756. (d) Herrera, J. M.; Ward, M. D.; Adams, H.; Pope, S. J. A.; Faulkner, S. *Chem. Commun.* **2006**, 1851. (e) Liu, B.; Li, B. L.; Li, Y. Z.; Chen, Y.; Bao, S. S.; Zheng, L. M. *Inorg. Chem.* **2007**, *46*, 8524.

(6) (a) Wu, C. D.; Lu, C. Z.; Zhuang, H. H.; Huang, J. S. *J. Am. Chem. Soc.* **2002**, *124*, 3836. (b) Li, F. Y.; Xu, L.; Weim, Y. G.; Gao, G. G.; Fan, L. H.; Li, Z. K. *Inorg. Chim. Acta* **2006**, *359*, 3795. (c) Chen, W. L.; Li, Y. G.; Wang, Y. H.; Wang, E. B. *Eur. J. Inorg. Chem.* **2007**, 2216.

(7) (a) Goodgame, D. M. L.; Müller, T. E. D.; Williams, J. *Polyhedron* **1992**, *11*, 1513. (b) Brouca-Cabarrecq, C.; Fave, O.; Mosset, A. *J. Chem. Cryst.* **1999**, *29*, 81. (c) Liang, Y. C.; Cao, R.; Su, W. P.; Hong, M. C. *Chem. Lett.* **2000**, 868. (d) Zhao, B.; Chen, X. Y.; Wang, W. Z.; Cheng, P.; Ding, B.; Liao, D. Z.; Yan, S. P.; Jiang, Z. H. *Inorg. Chem. Commum.* **2005**, *8*, 178. (e) Gu, X. J.; Xue, D. F. *Cryst. Growth Des.* **2006**, *6*, 2551. (f) Gu, X. J.; Xue, D. F. *Inorg. Chem.* **2006**, *45*, 9257. (g) Gu, X. J.; Xue, D. F. *CrystEngComm.* **2007**, *9*, 471. (h) Qiu, Y. C.; Liu, H. G.; Ling, Y.; Deng, H.; Zeng, R. H.; Zhou, G. Y.; Zeller, M. *Inorg. Chem. Commum.* **2007**, *10*, 1399. (i) Iki, N.; Ohta, M.; Horiuchi, T.; Hoshino, H. *Chem. Asian J.* **2008**, *3*, 849. (j) Liu, Z. H.; Qiu, Y. C.; Li, Y. H.; Peng, G.; Liu, B.; Deng, H. *Inorg. Chem. Commun.* **2009**, *12*, 204.

(8) (a) Zhao, B.; Zhao, X. Q.; Chen, Z.; Shi, W.; Cheng, P.; Yan, S. P.; Liao, D. Z. *CrystEngComm* **2008**, *10*, 1144. (b) Zhao, X. Q.; Zhao, B.; Shi, W.; Cheng, P. *CrystEngComm* **2009**, *11*, 1261.

(9) (a) Richardson, F. S. *Chem. Rev.* **1982**, *82*, 541. (b) Ma, L.; Evans, O. R.; Foxman, B. M.; Lin, W. B. *Inorg. Chem.* **1999**, *38*, 5837. (c) de Sá, G. F.; Malta, O. L.; Mello Donegá, de C.; Simas, A. M.; Longo, R. L.; Santa-Cruz, P. A.; da Silva, E. F., Jr. *Coord. Chem. Rev.* **2000**, *196*, 165. (d) Zebret, S.; Dupont, D.; Bernardinelli, G.; Hamack, J. *Chem.—Eur. J.* **2009**, *15*, 3358.

(10) (a) Fabbrizzi, L.; Licchelli, M.; Pallavicini, P. *Acc. Chem. Res.* **1999**, *32*, 846. (b) Glover, P. B.; Ashton, P. R.; Childs, L. J.; Rodger, A.; Kercher, M.; Williams, R. M.; Cola, L.; Pikramenou, Z. *J. Am. Chem. Soc.* **2003**, *125*, 9918. (c) Gunnlaugsson, T.; Leonard, J. P.; Senechal, K.; Harte, A. J. *J. Am. Chem. Soc.* **2003**, *125*, 12062. (d) Liu, W. S.; Jiao, T. Q.; Li, Y. Z.; Liu, Q. Z.; Tan, M. Y.; Wang, H.; Wang, L. F. *J. Am. Chem. Soc.* **2004**, *126*, 2280.

(11) Benelli, C.; Gatteschi, D. *Chem. Rev.* **2002**, *102*, 2369.

(12) For example: (a) Liu, S.; Gelmini, L.; Rettig, S. J.; Thompson, R. C.; Orvig, C. *J. Am. Chem. Soc.* **1992**, *114*, 6081. (b) Panagiotopoulos, A.; Zafiropoulos, T. F.; Perlepes, S. P.; Bakalbassis, E.; Masson-Ramade, I.; Kahn, O.; Teris, A.; Raptopoulou, C. P. *Inorg. Chem.* **1995**, *34*, 4918. (c) Costes, J. P.; Dahan, F.; Dupuis, A.; Lagrave, S.; Laurent, J. P. *Inorg. Chem.* **1998**, *37*, 153. (d) Dei, A.; Gatteschi, D.; Massa, C. A.; Pardi, S.; Poussereau, S.; Sorace, L. *Chem.—Eur. J.* **2000**, *6*, 4580. (e) Costes, J. P.; Dahan, F.; Nicodème, F. *Inorg. Chem.* **2001**, *40*, 5285. (f) Nishihara, S.; Akutagawa, T.; Hasegawa, T.; Nakamura, T. *Inorg. Chem.* **2003**, *42*, 2480. (g) Roy, L. E.; Hughbanks, T. *J. Am. Chem. Soc.* **2006**, *128*, 568.

(13) (a) Costes, J. P.; Clemente-Juan, J. M.; Dahan, F.; Nicodème, F.; Verelst, M. *Angew. Chem., Int. Ed.* **2002**, *41*, 323. (b) Hatscher, S. T.; Urland, W. *Angew. Chem., Int. Ed.* **2003**, *42*, 2862. (c) Hernández-Molina, M.; Ruiz-Pérez, C.; López, T.; Lloret, F.; Julve, M. *Inorg. Chem.* **2003**, *42*, 5456. (d) Costes, J. P.; Juan, J. M. C.; Dahan, F.; Nicodeme, F. *Dalton Trans.* **2003**, 1272. (e) Hou, H. W.; Li, G.; Li, L. K.; Zhu, Y.; Meng, X. R.; Fan, Y. T. *Inorg. Chem.* **2003**, *42*, 428. (f) Chen, Z.; Zhao, B.; Cheng, P.; Zhao, X. Q.; Shi, W.; Song, Y. *Inorg. Chem.* **2009**, *48*, 3493. (g) Baggio, R.; Calvo, R.; Garland, M. T.; Pena, O.; Perec, M.; Rizzi, A. *Inorg. Chem.* **2005**, *44*, 8979.

Table 1. Crystallographic Data for **1**−**5**

	1	**2**	**3**	**4**	**5**
formula	$LaAg_2C_{14}H_9N_2O_{12}$	$PrAgC_{14}H_{12}N_2O_{13}$	$NdAgC_{14}H_{12}N_2O_{13}$	$SmAgC_{14}H_{12}N_2O_{13}$	$EuAgC_{14}H_{12}N_2O_{13}$
M [g]	751.88	665.04	668.37	674.48	676.09
cryst syst	monoclinic	monoclinic	monoclinic	monoclinic	monoclinic
space group	$P2_1/n$	$C2/c$	$C2/c$	$C2/c$	$C2/c$
a [Å]	7.659(2)	8.0219(14)	8.0280(12)	8.0304(18)	8.0281(10)
b [Å]	13.348(4)	10.4085(17)	10.3957(15)	10.371(2)	10.3800(14)
c [Å]	17.469(5)	20.852(4)	20.766(3)	20.604(5)	20.589(3)
γ [deg]	100.539(4)	99.617(2)	99.657(2)	99.676(4)	99.748(2)
V [Å^3]	1755.8(8)	1716.6(5)	1708.5(4)	1691.5(6)	1690.9(4)
Z	4	4	4	4	4
ρ_{calcd} [g cm^{-3}]	2.844	2.573	2.598	2.649	2.656
μ [mm^{-1}]	4.674	4.029	4.235	4.680	4.918
$F(000)$	1416	1280	1284	1292	1296
$2\theta_{max}$ [deg]	50.04	52.72	50.04	50.04	52.54
limiting indices	$-9 \le h \le +9$	$-10 \le h \le +10$	$-7 \le h \le +9$	$-9 \le h \le +6$	$-8 \le h \le +9$
	$-7 \le k \le +15$	$-7 \le k \le +12$	$-12 \le k \le +12$	$-12 \le k \le +11$	$-12 \le k \le +12$
	$-20 \le l \le +20$	$-26 \le l \le +22$	$-24 \le l \le +20$	$-24 \le l \le +19$	$-19 \le l \le +24$
reflns collected/unique	8701/3079	4724/1743	4239/1511	4218/1501	4188/1501
data/restraints/params	3079/21/307	1743/2/155	1511/3/144	1501/3/144	1501/4/144
GOF on F^2	1.036	1.078	1.059	1.039	1.156
R_1/wR_2 [$I > 2\sigma(I)$]	0.0261/0.0627	0.0254/0.0573	0.0203/0.0458	0.0198/0.0467	0.0233/0.0576
R_1/wR_2 (all data)	0.0303/0.0645	0.0292/0.0585	0.0229/0.0468	0.0229/0.0480	0.0250/0.0585
largest diff. peak/hole (eÅ^{-3})	1.327/−1.108	1.351/−2.040	0.645/−0.491	0.608/−0.835	0.590/−1.403

and then cooled to room temperature at a rate of 5 °C h^{-1}. Colorless crystals of **1** were obtained in 63% yield based on La after being washed several times by water and diethyl ether. Anal. Calcd for **1**: C, 22.36; H, 1.21; N, 2.73. Found: C, 22.55; H, 1.42; N, 2.96.

Preparation of $\{LnAg(HCAM)_2(H_2O)_3\}_n$ (Ln = Pr, 2; Nd, 3; Sm, 4; Eu, 5) and $\{LnAg_3(CAM)_2(H_2O)\}_n$ (Ln = Gd, 6; Tb, 7; Dy, 8; Tm, 9; Yb, 10). These polymers were obtained following the method described above for **1**. The yields based on Ln were 72% (**2**), 70% (**3**), 59% (**4**), 50% (**5**), 60% (**6**), 58% (**7**), 62% (**8**), 55% (**9**), and 63% (**10**), respectively. Anal. Calcd for **2**: C, 25.28; H, 1.82; N, 4.21. Found: C, 24.56; H, 1.90; N, 4.88. Calcd for **3**: C, 25.16; H, 1.80; N, 4.19. Found: C, 24.63; H, 1.88; N, 4.32. Calcd for **4**: C, 24.93; H, 1.79; N, 4.15. Found: C, 24.52; H, 2.11; N, 4.23. Calcd for **5**: C, 24.87; H, 1.79; N, 4.14. Found: C, 24.26; H, 1.94; N, 4.33. Calcd for **6**: C, 19.57; H, 0.70; N, 3.26. Found: C, 19.12; H, 0.88; N, 3.55. Calcd for **7**: C, 19.54; H, 0.70; N, 3.25. Found: C, 19.11; H, 1.02; N, 3.56. Calcd for **8**: C, 19.45; H, 0.70; N, 3.24. Found: C, 19.03; H, 0.90; N, 3.63.; Calcd for **9**: C, 19.31; H, 0.69; N, 3.22. Found: C, 19.13; H, 0.82; N, 3.53. Calcd for **10**: C, 19.22; H, 0.69; N, 3.20. Found: C, 18.96; H, 0.91; N, 3.62.

X-Ray Structure Studies. Single-crystal X-ray data on **1**−**10** were collected on a computer-controlled Bruker SMART 1000 CCD diffractometer equipped with graphite-monochromated Mo Kα radiation with a radiation wavelength of 0.71073 Å by using the ω-scan technique. Lorentz polarization and absorption corrections were applied. The structures were solved by direct methods and refined with full-matrix least-squares techniques using the SHELXS-97 and SHELXL-97 programs.[14] Anisotropic thermal parameters were assigned to all non-hydrogen atoms. The organic hydrogen atoms were generated geometrically; the hydrogen atoms of the water molecules were located from different maps and refined with isotropic temperature factors. Analytical expressions of neutral-atom scattering factors were employed, and anomalous dispersion corrections were incorporated. The crystallographic data and structure refinement for **1**−**10** are listed in Tables 1 and 2, respectively.

CCDC-661616 (**1**), CCDC-661615 (**2**), CCDC-661617 (**3**), CCDC-661618 (**4**), CCDC-661619 (**5**), CCDC-661620 (**6**), CCDC-661621 (**7**), CCDC-662613 (**8**), CCDC-662611 (**9**), and CCDC-662612 (**10**) contain the supplementary crystallographic data for this paper. These data can be obtained free of charge from the Cambridge Crystallographic Data Centre via www.ccdc.cam.ac.uk/data_request/cif.

(14) (a) Sheldrick, G. M. *SHELXS-97*; University of Göttingen: Göttingen, Germany, 1997. (b) Sheldrick, G. M. *SHELXL-97*; University of Göttingen: Göttingen, Germany, 1997.

Results and Discussion

This series of compounds were synthesized by hydrothermal reaction of $Ln(OH)_3$, Ag_2O, and H_3CAM in a molar ratio of 1:1:3. The segregation into three structural types solely depends on the size of lanthanide ions, which demonstrates the lanthanide contraction effect. In the following, we describe the representatives for each structural type in detail and investigate their luminescent and magnetic properties.

Structural Analysis of $\{LaAg_2(CAM)(HCAM)(H_2O)_2\}_n$ (1). The single-crystal structural analysis reveals that **1** crystallizes in the monoclinic crystal system, space group $P2_1/n$. Each molecule contains two crystallographic independent Ag^+'s, one La^{3+}, one CAM^{3-}, one $HCAM^{2-}$, and two coordinated H_2O molecules. The coordination unit of **1** is shown in Figure 1, and both Ag1 and Ag2 are four-coordinated, while La1 is nine-coordinated. La1 links Ag1 and Ag2 through two carboxyl groups, respectively, and the Ag−Ag bond exists between Ag1 and Ag2 with a distance of 2.854(8) Å. The coordination environments of Ag1 and Ag2 are shown in Figure 2a, and both of them coordinate to one CAM and three HCAM anions to form a distorted tetrahedral geometry. Ag1 and Ag2 with two coordinated carboxyl groups form an Ag_2 unit with an eight-membered $Ag_2C_2O_4$ motif, and two neighboring Ag_2 units are connected through two HCAM anions to form a $[Ag_4(HCAM)_2]$ unit (Figure 2b). Each $Ag_4(HCAM)_2$ motif connects another four through CAM anions to form a highly ordered 2D layer (Figure 3a). The left carboxyl groups in HCAM anions and hydroxyl groups in CAM anions link the 2D layers (up and down) to form a 3D porous structure, as shown in Figure 3b. If considering the $[Ag_4(HCAM)_2]$ unit as a connecting node, the 2D layer can be interpreted as a 4^4 net with a distance between two nodes of 12.155 Å (Figure 3c), and the 3D framework can be simplified as an α-polonium-like topology with a distance

Table 2. Crystallographic Data for **6**−**10**

	6	**7**	**8**	**9**	**10**
formula	$GdAg_3C_{14}H_6N_2O_{11}$	$TbAg_3C_{14}H_6N_2O_{11}$	$DyAg_3C_{14}H_6N_2O_{11}$	$TmAg_3C_{14}H_6N_2O_{11}$	$YbAg_3C_{14}H_6N_2O_{11}$
M [g]	859.07	860.74	864.32	870.75	874.86
cryst syst	orthorhombic	orthorhombic	orthorhombic	orthorhombic	orthorhombic
space group	*Pnna*	*Pnna*	*Pnna*	*Pnna*	*Pnna*
a [Å]	8.2092(12)	8.2405(11)	8.2603(12)	8.2870(15)	8.296(3)
b [Å]	14.487(2)	14.5013(19)	14.530(2)	14.539(3)	14.545(5)
c [Å]	13.848(2)	13.8205(17)	13.796(2)	13.680(3)	13.647(5)
V [Å^3]	1646.8(4)	1651.5(4)	1655.8(4)	1648.3(5)	1646.6(9)
Z	4	4	4	4	4
ρ_{calcd} [g cm^{-3}]	3.465	3.462	3.467	3.509	3.529
μ [mm^{-1}]	7.564	7.809	8.030	8.916	9.217
$F(000)$	1588	1592	1596	1608	1612
$2\theta_{max}$ [deg]	52.82	52.72	52.86	50.04	52.90
limiting indices	$-10 \le h \le +5$ $-18 \le k \le +17$ $-17 \le l \le +16$	$-10 \le h \le +10$ $-15 \le k \le +18$ $-17 \le l \le +15$	$-10 \le h \le +10$ $-14 \le k \le +18$ $-15 \le l \le +17$	$-6 \le h \le +9$ $-17 \le k \le +12$ $-15 \le l \le +16$	$-10 \le h \le +8$ $-17 \le k \le +18$ $-17 \le l \le +16$
reflns collected/unique	8612/1692	8549/1676	8663/1703	7706/1450	8560/1690
data/restraints/params	1693/0/142	1676/0/142	1703/0/142	1450/0/143	1690/0/143
GOF on F^2	1.031	1.091	1.067	1.093	1.086
R_1/wR_2 [$I > 2\sigma(I)$]	0.0251/0.0545	0.0306/0.0734	0.0257/0.0574	0.0464/0.1177	0.0319/0.0750
R_1/wR_2 (all data)	0.0379/0.0581	0.0352/0.0757	0.0348/0.0604	0.0502/0.1205	0.0403/0.0791
largest diff. peak/hole (eÅ^{-3})	1.230/−1.342	1.514/−1.712	1.597/−1.302	3.309/−2.483	2.039/−1.376

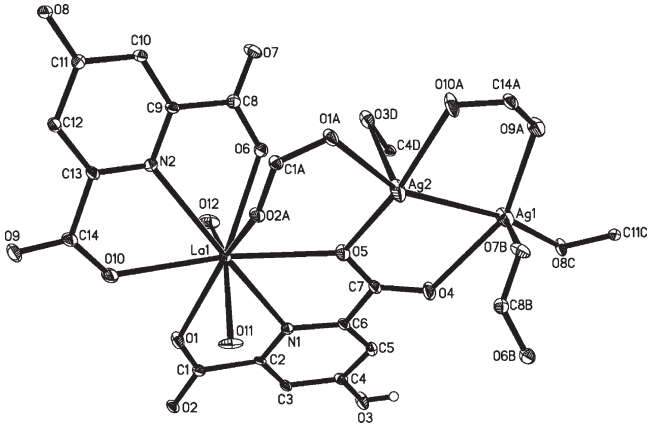

Figure 1. Coordination unit of **1**.

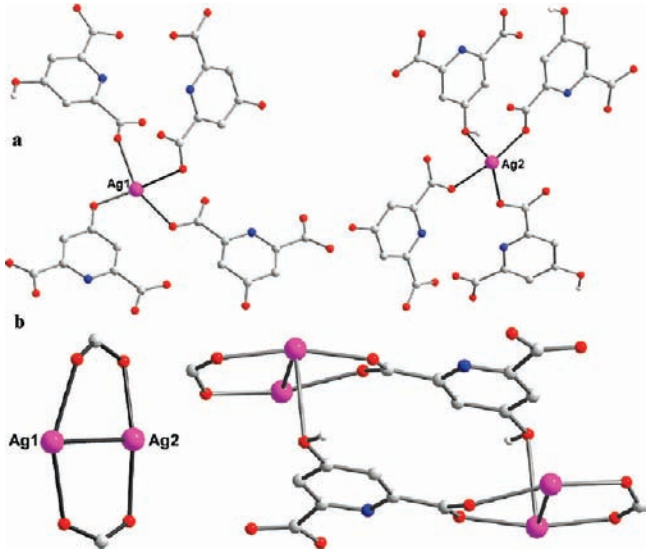

Figure 2. (a) Coordination environment of two kinds of Ag^+ ions in **1**. (b) Eight-membered $Ag_2C_2O_4$ motif and $Ag_4(HCAM)_2$ unit. Color codes: purple, Ag; red, O; blue, N; gray, C; white, H.

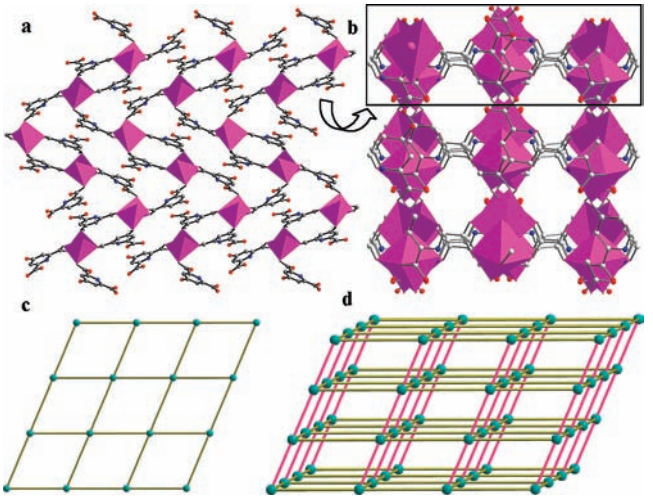

Figure 3. (a) Layer constructed of $Ag_4(HCAM)_2$ motifs along the *ac* plane in **1**. (b) The 3D porous framework containing Ag^+ ions in **1**. (c) The 4^4-net and (d) the α-polonium-like topology considering the $Ag_4(HCAM)_2$ motif as a connecting node. Color codes: purple polyhedral, $[AgO_4]$; red, O; blue, N; gray, C; cyan, $[Ag_4(HCAM)_2]$; red lines, linkage between Ag^+ layers.

between two layers of 7.659 Å (Figure 3d). The neighboring La^{3+} ions are connected through carboxyl bridges from HCAM anions to form the right- and left-handed (**P**/**M**) helical chains with La−OCO−La connectivity (Figure 4), and the pitch of each helix is 13.348 Å. The **P**- and **M**-type helices are arrayed alternately in the α-polonium-like Ag^+ net (Figure 5) and display the achirality of this structure. The helical chains containing La^{3+} ions and the 3D Ag^+ net are linked through HCAM and CAM bridges which coordinate with two kinds of metal ions to construct the whole 3D network.

Structural Analyses of $\{LnAg(HCAM)_2(H_2O)_3\}_n$ (Ln = Pr, 2; Nd, 3; Sm, 4; Eu, 5). X-ray crystallography has established that **2**−**5** are isomorphous and crystallize in monoclinic space group $C2/c$. Here, **2** is taken as a representative to depict this structure in detail. The

coordination environments of Pr^{3+} and Ag^{+} ions are shown in Figure 6a. The Pr1 atom coordinates to two tridentate HCAM anions and three H_2O molecules to form a $[PrN_2O_7]$ polyhedron. The coordination geometry around Ag1 is an antiprism consisting of six O atoms, and two trigonal planes both comprise two carboxylate O atoms and one bridging H_2O molecule. There is one crystallographically independent HCAM anion in this structure, which tridentately chelates to one Pr^{3+} and links two Ag^{+}'s. All Pr^{3+} and Ag^{+} are connected alternately by carboxylate O or H_2O bridges and generate a hexanuclear heterometallic Pr_3Ag_3 unit with an 18-membered $Pr_3Ag_3O_{12}$ motif (Figure 6b). The distances between adjacent Pr^{3+} and Ag^{+} are 4.091 (Pr1···Ag1) and 4.397 (Pr1A···Ag1) Å, and those of Pr···Pr and Ag···Ag are 6.571 (Pr1···Pr1A or Ag1···Ag1B) and 8.022 (Pr1A···Pr1B or Ag1···Ag1C) Å. Each Pr^{3+} has three Ag^{+}'s as the nearest metal centers, while every Ag^{+} also has three Pr^{3+}'s in its vicinity. As a result of this connection, the Pr_3Ag_3 hexagonal structure as a building block is further assembled into an analogous 2D honeycomb, and in this structure, all Pr^{3+} and Ag^{+} are coplanar (Figure 7). The uncoordinated hydroxyl groups provide rich hydrogen bonding donor or acceptor sites in the construction of supramolecular packing, and then the 2D honeycomb is further linked to a 3D supramolecular structure through hydrogen-bonding interactions with an −ABAB− sequence along the *b* axis (Figure 8). The distances of O···O and the angles of O−H···O of **2**−**5** are listed in Table 3.

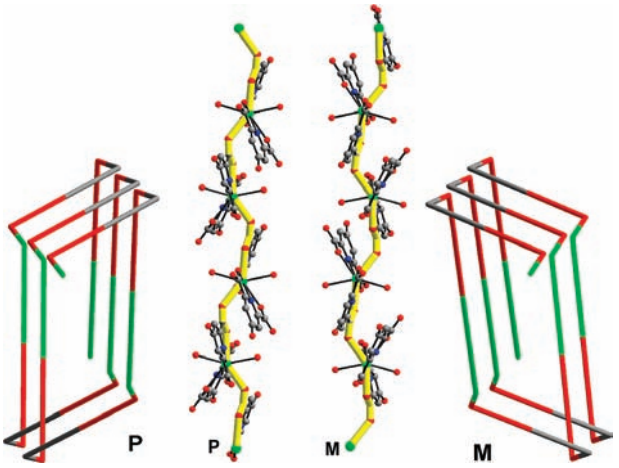

Figure 4. R/L helical chains consisting of La^{3+} ions with La−OCO−La connectivity (yellow) in **1**. Color codes: green, La; purple, Ag; red, O; blue, N; gray, C.

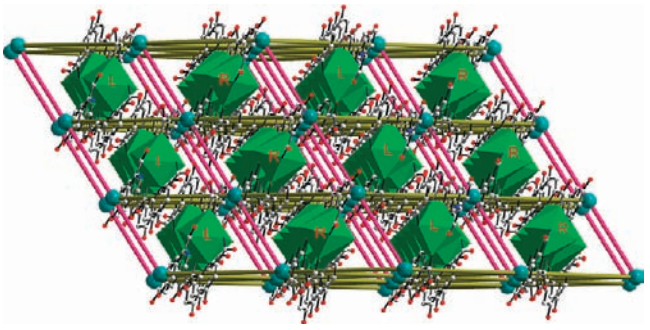

Figure 5. The 3D framework of **1** consisting of a 3D framework with Ag^{+} ions and 1D helical chains with La^{3+} ions. Color codes: green polyhedra, $[LaN_2O_7]$; cyan, $[Ag_4(HCAM)_2]$; red, O; blue, N; gray, C; red lines, linkers between Ag^{+} layers.

Structural Analyses of $\{LnAg_3(CAM)_2(H_2O)\}_n$ (Ln = Gd, 6; Tb, 7; Dy, 8; Tm, 9; Yb, 10). The X-ray analysis reveals that **6**−**10** are isostructural and crystallize in the orthorhombic system, space group *Pnna*. The overall structure displays a 3D framework fabricated by a 3D Ag^{+} net and 2D Ln^{3+}−4^4 layer. Compound **7** is taken as an example to depict the 3D structure in detail. There are

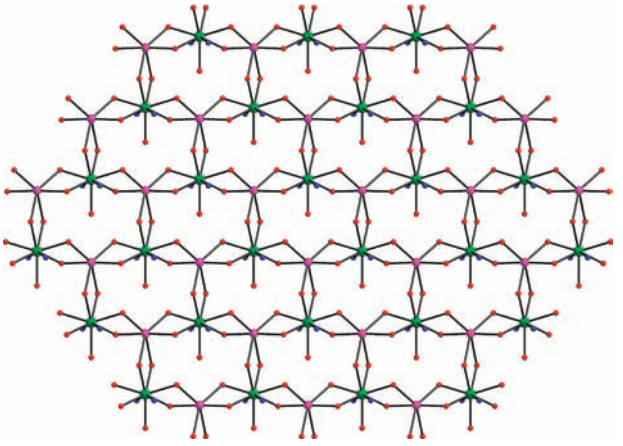

Figure 7. The 2D honeycomb-like structure of **2**. Color codes: green, Pr; purple, Ag; red, O; blue, N. C and H atoms are omitted for clarity.

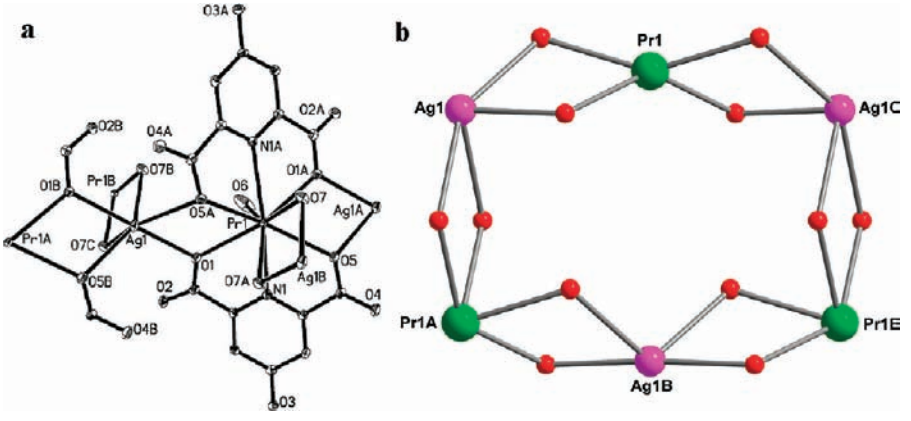

Figure 6. (a) Diagram showing the coordination environments of Pr^{3+} and Ag^{+} ions in **2**. (b) $Pr_3Ag_3O_{12}$ motif. Color codes: green, Pr; purple, Ag; red, O.

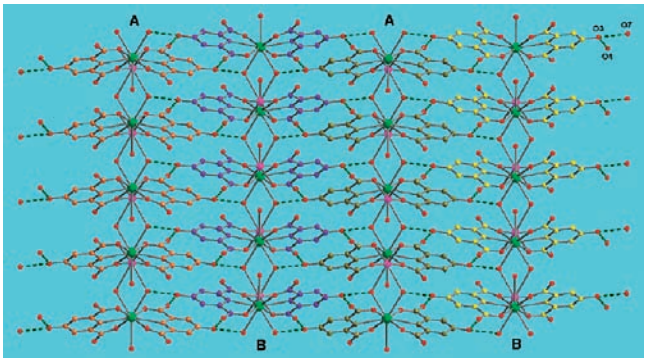

Figure 8. The packing structure constructed through hydrogen bonds with an −ABAB− sequence along the *a* direction of **2**. Color codes: green, Pr; purple, Ag; red, O; other colors, different atoms with O in order to highlight the hydrogen bonds; olive dot line, O···O hydrogen bonds. H atoms are omitted.

Table 3. O···O Distances and the Angles of O−H···O of Hydrogen Bonds in **2**−**5**

		2	**3**	**4**	**5**
O3−H···O4	O···O distance (Å)	2.632	2.629	2.626	2.619
hydrogen bond	O−H···O angle (deg)	164.68	174.86	177.56	166.74
O7−H···O3	O···O distance (Å)	2.848	2.834	2.823	2.833
hydrogen bond	O−H···O angle (deg)	157.04	157.14	144.65	161.12

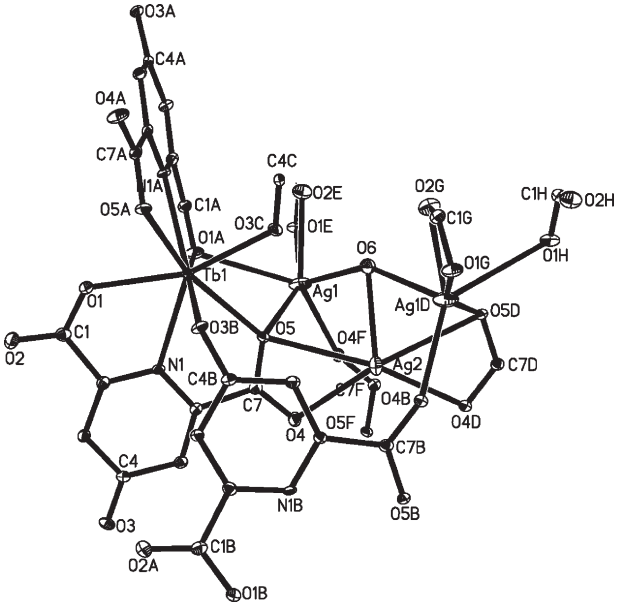

Figure 9. Coordination unit of **7**.

two crystallographically independent Ag^+'s, one Tb^{3+}, and one CAM anion in an asymmetric unit. Ag^+ ions have both six-coordinated (Ag1) and five-coordinated (Ag2) environments, and the Tb^{3+} ion is eight-coordinated with four CAM anions, as shown in Figure 9. Three Ag^+'s (Ag1, Ag2, Ag1D) are bridged by one μ_3-O atom (O_6). The Tb1 atom connects Ag1 and Ag2 through two carboxylate O atoms (O1A, O5), while Tb1 and Ag1D are connected through one CAM ligand. The Ag1 atom coordinates to five carboxyl O atoms and one H_2O molecule to form the antiprism coordination geometry, and the Ag2 atom coordinates to two carboxyl groups and one H_2O molecule to complete the planar-like geometry (Figure 10a). Each Ag2 atom links four Ag1 atoms through two carboxyl bridges. Ag1 and Ag1A are linked by one H_2O bridge, while Ag1B and Ag1C are bridged by two carboxylate O atoms. As a result of this connection, a $[Ag_5]$ unit with a 14-membered $Ag_5C_2O_7$ motif is built (Figure 10a). The shortest distances of Ag1···Ag2 and Ag1···Ag1 are 3.097 and 3.229 Å, respectively. The building block $[Ag_5]$ structure using Ag1 atoms as noted is further assembled into a 1D ribbon (Figure 10b). Each ribbon links four others through CAM anions to form a 3D porous Ag^+ net. There are two types of pores existing in the Ag^+ net: the first one is formed by two ribbons, and the second one is formed by four ribbons, as shown in Figure 10c. CAM anions as quadridentate ligands link Tb^{3+} ions to form a highly ordered 2D 4^4 net, as shown in Figure 11a. The 4^4 nets are inserted into the 3D Ag^+ net (Figure 11b) through coordination bonds, and the result is a sandwich-like 3D network (Figure 9c).

Structural Changes in Ln−Ag−CAM Series. The coordination geometries of lanthanide ions and the overall networks in **1**−**10** change regularly with the contraction of lanthanide ions in radius. Compound **1**, containing the large La atom, consists of a 3D framework which is different from other compounds, and the coordination number of the La atom is nine. Compounds **2**−**5** containing the intermediate ones (Pr−Eu) are converted to 2D polymers with an analogous honeycomb structure, while the coordination number of Ln atoms is still nine. Compounds **6**−**10** with the small ones (Gd−Dy, Tm, Yb) are 3D coordination polymers; moreover, the coordination number of Ln atoms becomes eight. The different coordination modes of ligands (Chart 2) result in the flexibility of the structures. There are both CAM and HCAM anions with coordination modes **A** and **B** existing in **1**; furthermore, all hydroxyl groups (dehydrogenated or hydrogenated) coordinate with Ag^+ ions. In **2**−**5**, only HCAM anions with coordination mode **C** exist, in which the hydroxyl groups (hydrogenated) are uncoordinated. CAM anions with coordination mode **D** are found in **6**−**10**, and the hydroxyl groups (dehydrogenated) coordinate with Ln^{3+} ions. It is clear that with the contraction of lanthanide ions in radius, the coordination number of the Ln atoms changes from nine to eight, and the overall structures go from a 3D framework to a 2D honeycomb and then to a sandwich-like 3D network.

Interestingly, strong silver−silver interactions are observed in compounds **1** and **6**−**10**. The Ag−Ag distance in **1** is 2.854(8) Å and is slightly shorter than that in metallic silver, which has been reported as 2.89 Å.[15] The Ag···Ag distances in compounds **6**−**10** range from 3.101 to 3.074 Å (Table 4), between that of metallic silver and the sum of van der Waals radii of 3.44 Å.[16] Those short Ag−Ag distances reveal significant metal−metal interactions in compounds **1** and **6**−**10**.

Compounds **2**−**5** and **6**−**10** are isomorphous, respectively. Various crystal lattice constants of these isomorphous compounds clearly exhibit the lanthanide

(15) (a) Jensen, M. *Angew. Chem., Int. Ed. Engl.* **1987**, *26*, 1098. (b) Wells, A. F. *Structural Inorganic Chemistry*, 5th ed.; Clarendon Press: London, 1984, 1098.

(16) Bondi, A. *J. Phys. Chem.* **1984**, *6*, 441.

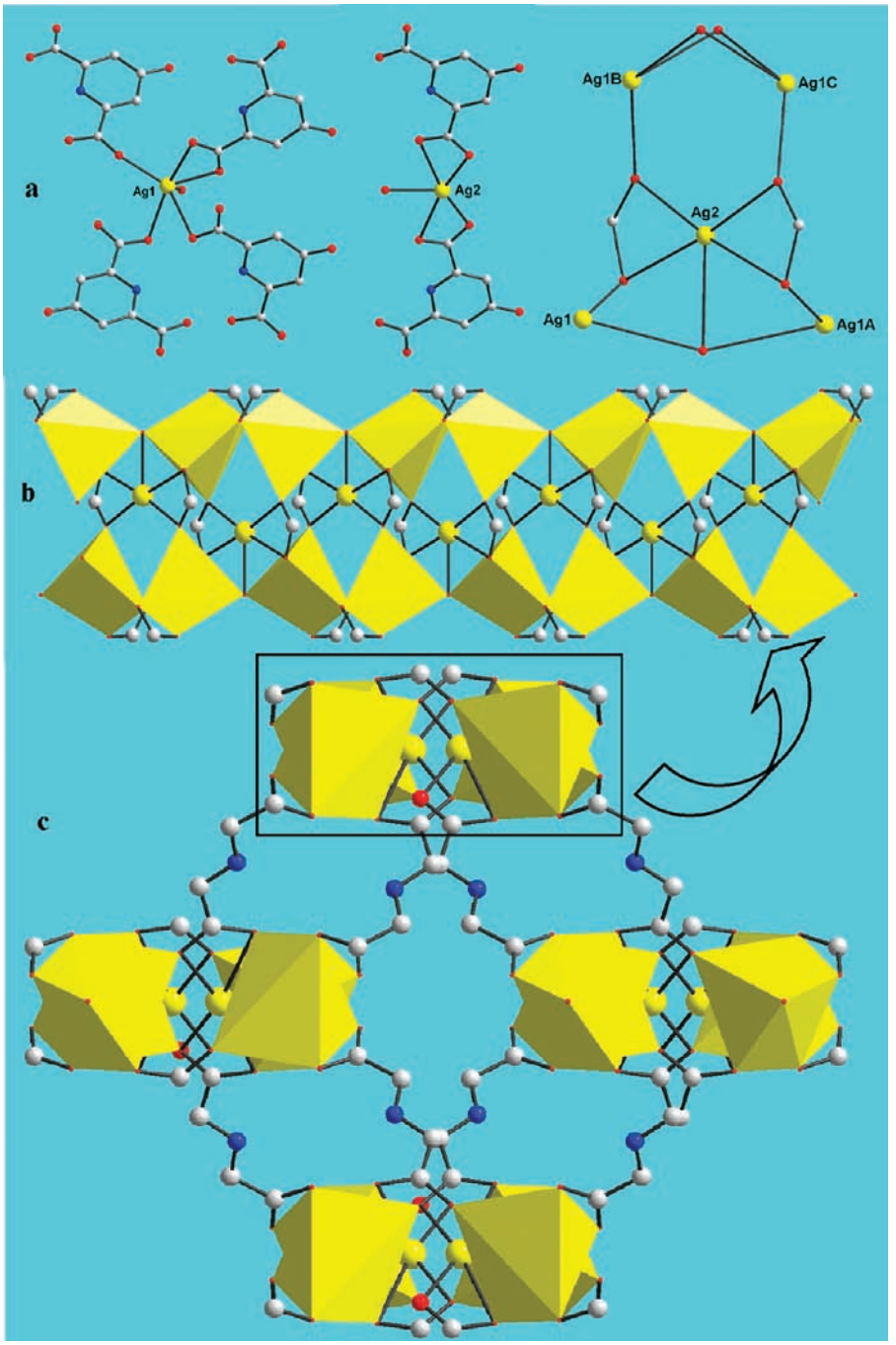

Figure 10. (a) Coordination environments of Ag1 and Ag2 ions and the connectivity of Ag1 and Ag2 ions in **7**. (b) The 1D chain and (c) 3D porous structure consisting of Ag^+ ions in **7**. Color codes: yellow, Ag2; red, O; blue, N; gray, C; yellow polydedra, [$Ag1O_6$]. Some C and H atoms are omitted for clarity.

contraction effect. As shown in Table 4, the Ln−O_W, Ln−O_C, and Ln−N distances decrease from Pr to Eu, which can be ascribed to the lanthanide contraction effect. The same trend is observed in Ln−O_H, Ln−O_C, and Ln−N bond lengths of compounds **6**−**10** (from Gd to Yb), and the Ln···Ln distances also decrease from 8.049 (Gd···Gd) to 7.985 Å (Yb···Yb).

Structural Comparison with Ln−Ag−PDA Series. The stereochemical and supramolecular effects of the hydroxyl group in H_3CAM result in dramatic structural differences from those of the Ln−Ag−PDA series reported previously,[8] as shown in Scheme 1. The Ln−Ag−PDA series contain three kinds of structures: the products of the Pr ion exhibit a 2D grid structure; those containing Ce−Dy (except Pr) ions construct an achiral double-helical chain; that containing the Er^{3+} ion is an infinite triple-stranded helical polymer, in which the right- and left-handed helices array alternately and are indicative of achirality of this compound. The structural progression in the Ln−Ag−CAM series can be solely ascribed to the effect of lanthanide contraction, and the overall frameworks change regularly with the increasing number of lanthanide ions. In the Ln−Ag−PDA series, the complex with Pr stands out from those with Ce−Dy lanthanides

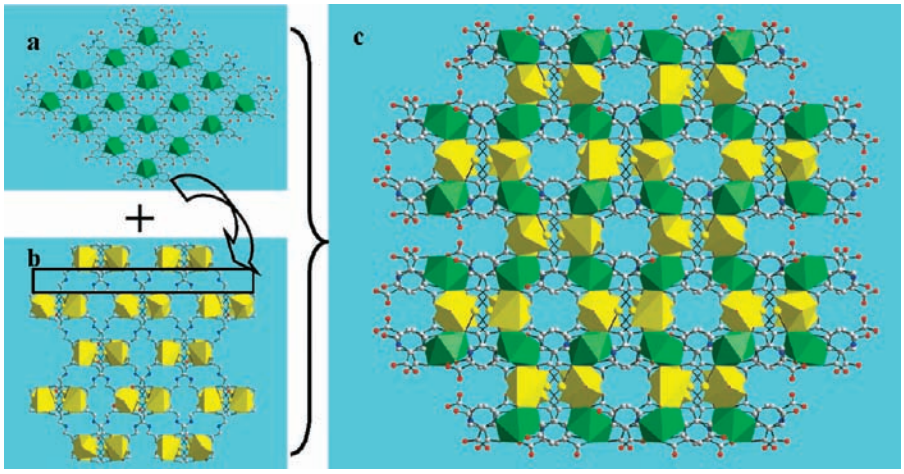

Figure 11. The 3D framework (a) containing Ag^+ ions and a 2D grid (b) with Tb^{3+} ions constructed in a 3D network (c) in **7**. Color codes: yellow, Ag2; red, O; blue, N; gray, C; green polyhedra, [TbN_2O_6]; yellow polyhedra, [$Ag1O_6$].

Chart 2. Coordination Modes of CAM and HCAM Ligands Observed in Ln−Ag−CAM Series

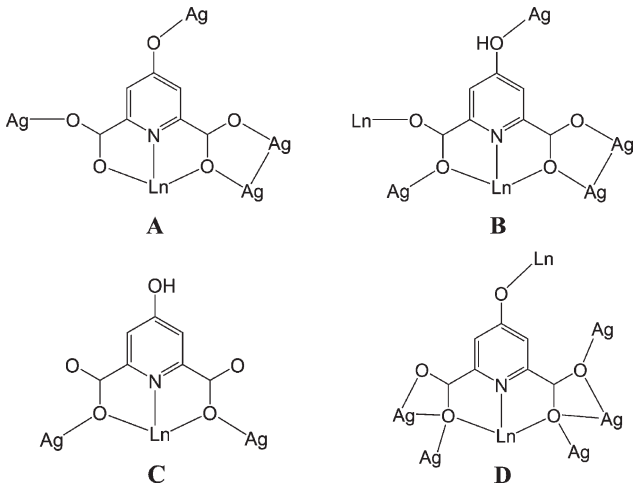

Table 4. Average Bond Lengths Associated with Ln Atoms and the Ag···Ag Distances (Å) of **2**−**10**[a]

	2	**3**	**4**	**5**	**6**	**7**	**8**	**9**	**10**
Ln−O_W	2.548	2.527	2.494	2.481					
Ln−O_H					2.336	2.317	2.307	2.274	2.256
Ln−O_C	2.510	2.496	2.496	2.462	2.439	2.429	2.422	2.382	2.382
Ln−N	2.596	2.577	2.543	2.528	2.496	2.488	2.478	2.447	2.423
Ln···Ln					8.049	8.045	8.040	7.997	7.985
Ag···Ag					3.101	3.097	3.094	3.076	3.074

[a] O_H, oxygen atom of the hydroxyl group; O_W, oxygen atom of the coordinated water molecule; O_C, oxygen atom of the carboxyl group.

(1D chain) and shows a 2D grid structure, which exhibits irregularity. It is obvious that the existence of a hydroxyl group makes the coordination modes of CAM ligands (Chart 2) more complicated than those of PDA ligands,[8] which directly result in high-dimensional structures (3D). By contrast, the Ln−Ag−PDA series only contains one 2D polymer, while other series are 1D chains. Even if the hydroxyl group is uncoordinated, the result is a highly ordered 2D layer; it shows that the stereochemical effect of the hydroxyl group plays an important role in the construction of the highly ordered 2D honeybomb-like structures (**2**−**5**) in the Ln−Ag−CAM series.

Compared to H_2PDA in the Ln−Ag−PDA series, with the H_3CAM units, using the hydroxyl group at the 4 position of H_2PDA to construct the Ln−Ag−CAM series has two advantages. First, if the hydroxyl group coordinates with metal ions, products tend to form a three-dimensional structure, such as **1** and **6**−**10**. Furthermore, the most important point is that Ln^{3+} ions are connected to form a 2D layer in **6**−**10**, and then it is possible to study the magnetic interactions among Ln^{3+} ions. The second advantage is that, even if the hydroxyl group is uncoordinated, the stereochemical effect of the hydroxyl group makes the result regularly ordered, such as **2**−**5** in the Ln−Ag−CAM series.

Luminescent Properties. The solid-state emission spectra of **4**, **5**, **7**, and **8** at room temperature are shown in Figure 12. When excited at 305 nm, **4** exhibits three characteristic transitions of the Sm^{3+} ion: 564, 598−608, and 644 nm, which is ascribed to $^4G_{5/2} \rightarrow {}^6H_J$ ($J = 5/2$ to $9/2$).[17] The $^4G_{5/2} \rightarrow {}^6H_{7/2}$ transition is around 602 nm, which is split into two bands at 598 and 608 nm, and the $^4G_{5/2} \rightarrow {}^6H_{9/2}$ transition around 644 nm consists of an intense peak with one weak shoulder. Compound **5** emits red light (excited at 290 nm), which arises from the $^5D_0 \rightarrow {}^7F_J$ ($J = 1-4$; 598, 614, 649, and 700 nm) and $^5D_1 \rightarrow {}^7F_1$ (543 nm) transitions of the Eu^{3+} ion.[18] The strongest emission is the $^5D_0 \rightarrow {}^7F_2$ transition, which is an electric dipole transition. Although the magnetic dipole transition of $^5D_0 \rightarrow {}^7F_1$, which is fairly insensitive to the coordination environment of the Eu^{3+} ion, is also present, it is clearly less intense than the $^5D_0 \rightarrow {}^7F_2$ transition. This indicates the absence of inversion symmetry at the Eu^{3+} sites in **5**.[19] This is in agreement with the result of the single-crystal X-ray analysis. The shoulder peaks exist in $^5D_0 \rightarrow {}^7F_1$, $^5D_0 \rightarrow {}^7F_2$, and $^5D_0 \rightarrow {}^7F_4$ emissions.

(17) Bassett, A. P.; Magennes, S. W.; Glover, P. B.; Lewis, D. J.; Spencer, N.; Parsons, S.; Williams, R. M.; De Cola, L.; Pikramenou, Z. *J. Am. Chem. Soc.* **2004**, *126*, 9413.
(18) Vicentini, G.; Zinner, L. B.; Zukerman-Schpector, J.; Zinner, K. *Coord. Chem. Rev.* **2000**, *196*, 353.
(19) (a) Judd, B. R. *Phys. Rev.* **1962**, *127*, 750. (b) Ofelt, G. S. *J. Chem. Phys.* **1962**, *37*, 511. (c) Blasse, G.; Grabmaier, B. C. *Luminescent Materials*; Springer-Verlag: New York, 1994.

Scheme 1. Structural Differences in Ln−Ag−CAM and Ln−Ag−PDA Series

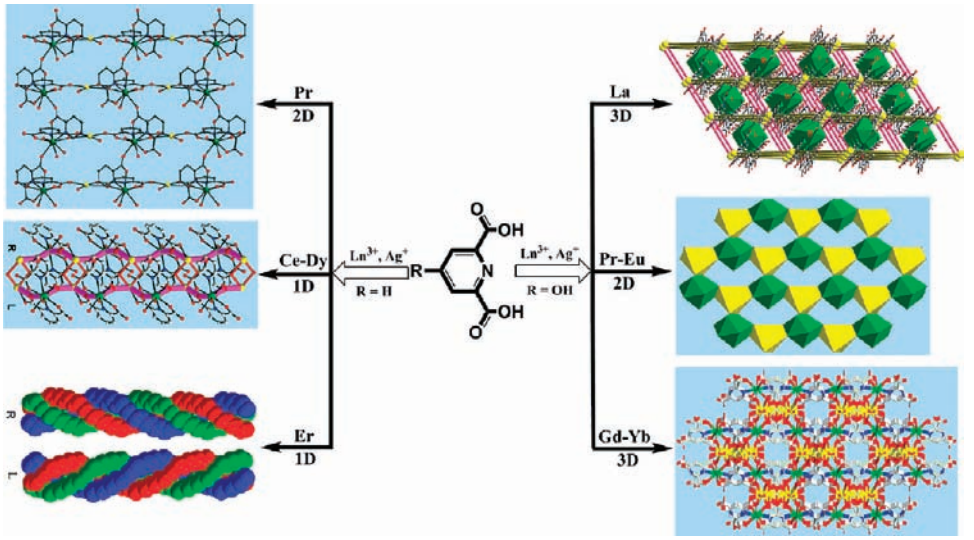

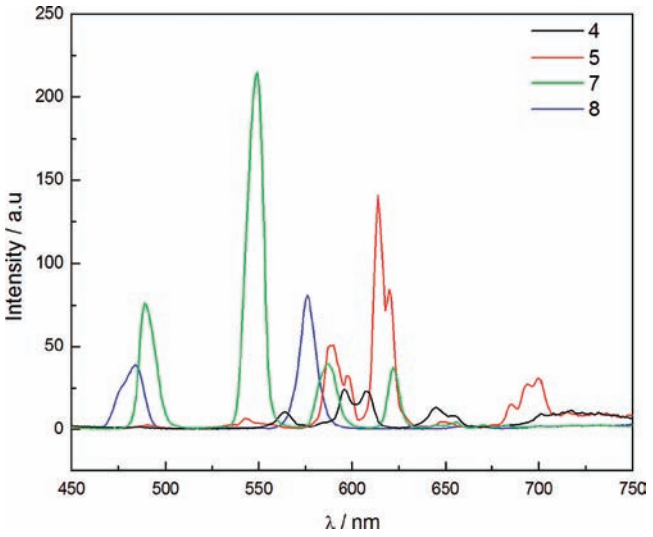

Figure 12. Solid-state emission spectra of **4** (excited at 305 nm), **5** (excited at 290 nm), **7** (excited at 324 nm), and **8** (excited at 320 nm) at room temperature.

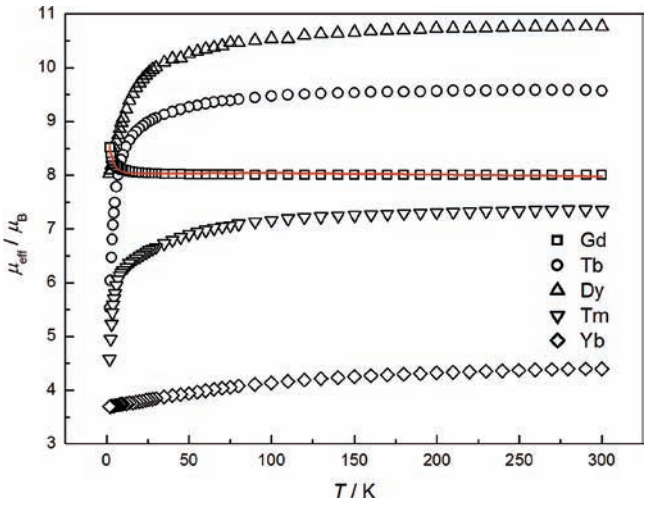

Figure 13. Temperature dependence of magnetic susceptibility in the form of μ_{eff} at an applied field of 1000 Oe from 2 to 300 K for compounds **6** (□), **7** (○), **8** (△), **9** (▽), and **10** (◇). The red line represents the best fit for **6** (see text).

Compound **7** yields intense green luminescence when excited at 324 nm. The emissions at 489, 548, 586, and 622 nm are assigned to the characteristic transitions of $^5D_4 \rightarrow {}^7F_J$ ($J = 6-3$) of the Tb^{3+} ion, respectively,[20] and the strongest emission is the $^5D_4 \rightarrow {}^7F_5$ transition (548 nm). When **8** is excited at 320 nm, a typical Dy^{3+} emission spectrum in the visible region exists.[21] Two dominant bands at 484 and 576 nm correspond to $^4F_{9/2} \rightarrow {}^6H_{15/2}$ and $^4F_{9/2} \rightarrow {}^6H_{13/2}$, respectively. The luminescent investigations on the four compounds (**4**, **5**, **7**, and **8**) mentioned above suggest that H_3CAM can effectively sensitize the luminescence of Sm^{3+}, Eu^{3+}, Tb^{3+}, and Dy^{3+} ions.

Magnetic Properties. According to the structure data described above, magnetic studies are performed for **6**−**10** in the 2−300 K range with a 1 KOe field to evaluate the possible exchange interactions among the lanthanide centers. Temperature dependence of the magnetic moments of **6**−**10** in the form of μ_{eff} versus T are shown in Figure 13. The field dependence of magnetization at 2 K for **6** is provided (Figure 14).

For **6**, the μ_{eff} value at 300 K is equal to 7.97 μ_B, which is consistent with the theoretical value for one insolated Gd^{3+} with $S = 7/2$ and $g = 2.0$. As the temperature is lowered, the magnetic moment increases until it reaches a maximum value of 8.55 μ_B at 2 K. This curve is typical of a weak but significant ferromagnetic exchange interaction between Gd^{3+}'s. Also, the magnetization curve supports the ferromagnetic nature of Gd···Gd interaction in **6**. There is only one possible exchange pathway (CAM bridges) between Gd^{3+} with a metal−metal separation of 8.049 Å. Here, we analyze the magnetic properties of **6** with a local spin of 7/2 by means of the analytical expression derived by Curély for an infinite 2D square lattice based on the exchange Hamiltonian $H = -\sum_{nn} JS_iS_j$, where $\sum_{nn}$ runs over all pairs of nearest-neighbor

(20) Tedeschi, C.; Azema, J.; Gornitzka, H.; Tisnes, P.; Picard, C. *Dalton Trans.* **2003**, 1738.
(21) Arnaud, N.; Vaquer, E.; Georges, *J. Analyst*. **1998**, *123*, 261.

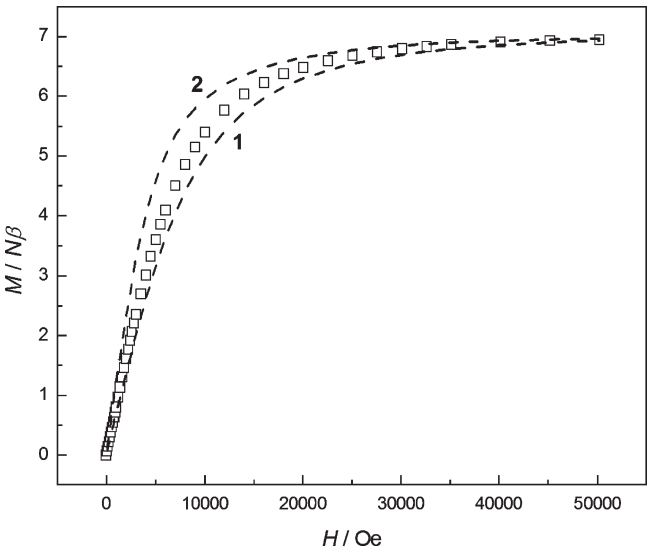

Figure 14. Field-independent magnetization for **6** at 2 K (□). The dashed lines represent the Brillouin function for (1) two uncoupled Gd centers and (2) an $S = 7$ state.

spins i and j (Heisenberg couplings):[22]

$$\chi = [Ng^2\beta^2 S(S+1)(1+u)^2]/[3kT(1-u)^2]$$

The best fit leads to $J = 0.004$ cm^{-1} and $g = 2.016$, and the agreement factor $R = \sum (\chi_m T_{obs} - \chi_m T_{calc})^2/\sum (\chi_m T_{calc})^2$ is 4.9×10^{-4}. This J value is comparable to that in reported gadolinium complex $[Gd_2L_6(MeOH)_2(H_2O)_2]\cdot 2MeOH\cdot 2H_2O$ (HL = ferrocenecarboxylate) of $J = 0.006$ cm^{-1} with a g value of 2.0.[13e,f]

The experimental magnetization curve at 2 K in the fields between 0 and 5 T is comprised between two calculated curves corresponding to the Brillouin functions for curve 1 (two isolated Gd^{3+} centers with $S = 7/2$, $g = 2.0$) and curve 2 (one system with $S = 7$, $g = 2.0$). In the high-field regime, single Gd^{3+} behavior is observed in curve 1 because of magnetic decoupling, and in the low-field regime, the measured values are shown in curve 2 for the ferromagnetic ground state (Figure 14).

For **7**−**10**, the magnetic behaviors show similar features, and the μ_{eff} values decrease with decreasing temperature. The observed μ_{eff} values of **7**−**10** at room temperature are 9.57, 10.77, 7.35, and 4.39 μ_B, which are close to the theoretical values of 9.72, 10.65, 7.56, and 4.54 μ_B for 1 M free Tb^{3+}, Dy^{3+}, Tm^{3+}, and Yb^{3+} ions, respectively. With the decreasing temperature, μ_{eff} continuously decreases to minimum values of 5.53, 8.03, 4.58, and 3.70 μ_B for **7**−**10**, respectively. Compared with the significant ferromagnetic exchange interaction between Gd^{3+}'s in **6**, it is very difficult to interpret the magnetic properties of **7**−**10**, because lanthanide ions of these systems have an orbital degenerate ground state which can cause the same feature. Usually, the interelectronic repulsion among 4f electrons and spin−orbital coupling lead to the $4f^n$ configuration of Ln^{3+} ions, except for the Gd^{3+} ion, to split into $^{2S+1}L_J$ states, and the latter further splits into Stark components, which is caused by the crystal-field perturbation.[23] At room temperature, all of the Stark levels arising from the n-fold degenerate $^{2S+1}L_J$ ground states of Ln^{3+} ions are thermally populated. As the temperature is lowered, a progressive depopulation of these levels occurs. As a result, the nature of interactions among Ln^{3+} ions in **7**−**10** cannot be distinctly deduced only from the μ_{eff} values smoothly decreasing on cooling.

Conclusion

In summary, we have successfully synthesized a new series of Ln−Ag heterometal−organic frameworks via hydrothermal reactions. With the increasing atomic number of lanthanide ions, the structures of **1**−**10** progress from a 3D framework (**1**) to honeycomb-like structures (**2**−**5**), and to sandwich-like 3D coordination polymers (**6**−**10**). The structural progression is mainly ascribed to the effect of lanthanide contraction, which is reflected not only in bonding and nonbonding interatomic distances but also in coordination number and geometry. The studies of luminescent properties show the typical luminescence of Sm^{3+} (**4**), Eu^{3+} (**5**), Tb^{3+} (**7**), and Dy^{3+} (**8**) ions in the visible region and indicate the efficient energy transfer from the CAM chromophore to lanthanide ions. Magnetic studies reveal that the ferromagnetic interaction appears among Gd^{3+} ions in **6**. The investigation of this series of Ln−Ag heterometallic frameworks may provide a rational synthetic strategy for the construction of lanthanide−traditional coordination polymer materials with novel luminescent and magnetic properties.

Acknowledgment. This work was supported by the National Natural Science Foundation of China (Grant 20631030, 20971074), FANEDD (200732), NCET-07-0463, and the State Key Project of Fundamental Research of MOST (Grant 2007CB815305).

Supporting Information Available: X-ray crystallographic files (CIF) of **1**−**10**. This material is available free of charge via the Internet at http://pubs.acs.org.

(22) (a) Curély, J. *Europhys. Lett.* **1995**, *32*, 529. (b) Curély, J. *Physica B* **1998**, *245*, 263. (c) Curély, J. *Physica B* **1998**, *254*, 277. (d) Curély, J.; Rouch, J. *Physica B* **1998**, *254*, 298.

(23) (a) Bunzli, J. C. G.; Chopin, G. R. *Lanthanide Probes in Life, Chemical and Earth Sciences*; Elsevier: Amsterdam, 1989. (b) Costes, J. P.; Nicodème, F. *Chem.—Eur. J.* **2002**, *8*, 3442.